Hyperbolic chaos in the klystron-type microwave vacuum tube oscillator

V. V. Emel'yanov, S. P. Kuznetsov, and N. M. Ryskin[a]
Saratov State University, Saratov 410012, Russia

The ring-loop oscillator consisting of two coupled klystrons which is capable of generating hyperbolic chaotic signal in the microwave band is considered. The system of delayed-differential equations describing the dynamics of the oscillator is derived. This system is further reduced to the two-dimensional return map under the assumption of the instantaneous build-up of oscillations in the cavities. The results of detailed numerical simulation for both models are presented showing that there exists large enough range of control parameters where the sustained regime corresponds to the structurally stable hyperbolic chaos. © *2010 American Institute of Physics*. [doi:10.1063/1.3494156]

Klystrons are well-known vacuum electron tubes widely used in communication and radar systems, particle accelerators, etc. In this paper, we consider the ring-loop oscillator consisting of two coupled klystrons which is capable of generating hyperbolic chaotic signal in the microwave band. The first klystron doubles the phase of the input signal. In the second klystron the second harmonic signal is mixed with the reference signal representing a periodic sequence of pulses with the third harmonic carrier frequency with subsequent extraction of the difference frequency signal. As a result, the transformation of the signal phase during the pulse period of the reference signal is described by a chaotic Bernoulli map. In a large enough range of control parameters the oscillator produces robust structurally stable chaotic signal insensitive to small variation of parameters. This is important for possible application in chaos-based communication and radar systems.

I. INTRODUCTION

The hyperbolic chaos is known as the strongest type of the chaotic behavior when the strange attractor is composed exclusively of trajectories of saddle type.[1] Such attractors possess the property of structural stability that implies insensitivity of the system dynamics and the attractor structure to variations of parameters and functions describing the system. Recently an approach for design of radio frequency oscillator with hyperbolic attractor has been proposed.[2,3] The operation principle of such system is alternating excitation of two coupled oscillators so that the transformation of the signal phase is described by chaotic Bernoulli map, which is a classical example of system with hyperbolic attractor.[1] Such generators are of practical interest for novel communication and radar systems using chaotic signals.[4,5]

In Ref. 6 we extended this principle to the microwave band using two coupled klystrons, which are widely used in communication and radar systems, particle accelerators, etc.[7–9] The scheme of the oscillator is presented in Fig. 1.

The input cavity of the first klystron is tuned to the frequency of ω, while the output one is tuned to frequency of 2ω. Thus, the first klystron doubles the frequency of the input signal. The output signal of the first klystron is fed to the input cavity of the second klystron via a wide-band dispersionless transmission line containing a phase shifter and an attenuator, which allow the signal phase and amplitude to be adjusted. In the second klystron, this signal is mixed with a reference signal, which represents a periodic sequence of pulses with carrier frequency of 3ω. Thus, in the second klystron there is a mixing of the signals of the second and third harmonics. In the output cavity of the second klystron a signal on a difference frequency of ω is separated and fed to the input cavity of the first klystron, thus closing the feedback circuit. The preliminary results of the numerical simulation[6] showed that at certain values of control parameters the generation of the hyperbolic chaotic signal is possible.

In this paper, we present the results of detailed analysis of the klystron microwave generator of hyperbolic chaos. In Sec. II a system of time-delayed differential equations describing the oscillator dynamics is derived. Under the assumption of the instantaneous build-up of oscillation in the cavities this system is reduced to a two-dimensional (2D) map for complex amplitude of the field. Numerical results for both models are presented in Secs. III and IV. We found the domain of control parameters where hyperbolic chaos is observed. In this domain, the dynamics of the phase of the oscillations is approximately described by the Bernoulli map, and as believed in the phase space an attractor of Smale–Williams type exists. To prove the hyperbolic nature of the chaotic signal, we calculate the largest Lyapunov exponent, which is almost insensitive to variation of parameters.

II. BASIC EQUATIONS

In Ref. 6 a system of dimensionless delay-differential equations (DDEs) describing the dynamics of the oscillator was presented

$$\dot{F}_1^\omega + F_1^\omega = \rho_2 e^{i\psi_2} F_2^\omega / \sqrt{2}, \tag{1}$$
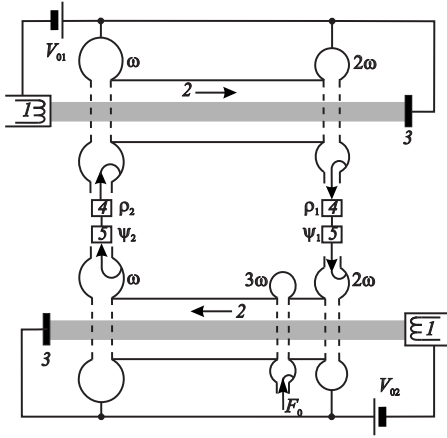
FIG. 1. Scheme of the proposed chaos generator based on coupled drift klystrons. *1*—electron guns, *2*—electron beams, *3*—collectors, *4*—variable attenuators, *5*—phase shifters.

$$\dot{F}_1^{2\omega} + \delta F_1^{2\omega} = 4\alpha_1 J_2(2|F_1^{\omega}(t-\tau)|)e^{2i(\varphi_1^{\omega}(t-\tau)-\theta_0)}, \tag{2}$$

$$\dot{F}_2^{2\omega} + \delta F_2^{2\omega} = \sqrt{2}\rho_1 e^{i\psi_1}F_1^{2\omega}, \tag{3}$$

$$\dot{F}_2^{\omega} + F_2^{\omega} = 2\alpha_2 e^{-i\theta_0}\sum_{m=-\infty}^{\infty} i^m J_{3m+1}(|F_2^{2\omega}(t-\tau)|)$$
$$\times J_{2m+1}(|F_2^{3\omega}(t)|)e^{-i(3m+1)\varphi_2^{2\omega}(t-\tau)}. \tag{4}$$

Here $F_j^{k\omega}(t)$ are dimensionless slowly varying complex amplitudes of the signals in corresponding cavities, $\varphi_j^{k\omega} = \arg(F_j^{k\omega})$, the subscripts $j=1,2$ henceforth indicate the number of klystrons, the superscripts $\omega, 2\omega$ denote the resonance frequencies of the cavities (see Fig. 1); $F_2^{3\omega}(t)$ is the normalized amplitude of the reference signal at third harmonic; τ is the normalized delay parameter; θ_0 is the unperturbed electron transit angle in the drift space; parameter $\delta = 2Q^{\omega}/Q^{2\omega}$ defines the ratio of Q-factors of the cavities operating at frequencies ω and 2ω; parameters ρ_j and ψ_j are attenuations and phase shifts in the coupling transmission lines, respectively; J_n is nth order Bessel functions of the first kind. The excitation parameters α_j, which can be treated as the normalized dc electron beam currents, most significantly influence the oscillator dynamics. Equations (1)–(4) are derived in a similar way as for other klystron-type delayed feedback oscillators.[10,11] Detailed derivation and description of parameters are presented in the Appendix.

Let the reference signal at the third harmonic frequency $F_2^{3\omega}(t)$ be supplied from an external driving source in the form of a sequence of pulses with constant amplitude F_0 and a repetition period equal to the time of signal passage via the feedback circuit 2τ. Assuming that the oscillation build-up in the cavities is fast in comparison with delay time one can neglect the derivatives in Eqs. (1)–(4) and obtain

$$F_1^{\omega} = \rho_2 e^{i\psi_2}F_2^{\omega}/\sqrt{2},$$

$$\delta F_1^{2\omega} = 4\alpha_1 J_2(2|F_1^{\omega}(t-\tau)|)e^{2i(\varphi_1^{\omega}(t-\tau)-\theta_0)},$$

$$\delta F_2^{2\omega} = \sqrt{2}\rho_1 e^{i\psi_1}F_1^{2\omega},$$
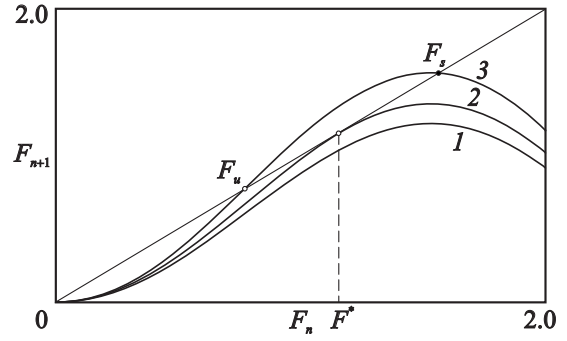
FIG. 2. Iterative diagram for the map (8) at different values of r: *1*—$r<r_c$; *2*—$r=r_c$; *3*—$r>r_c$.

$$F_2^{\omega} = 2\alpha_2 e^{-i\theta_0}\sum_{m=-\infty}^{\infty} i^m J_{3m+1}(|F_2^{2\omega}(t-\tau)|)$$
$$\times J_{2m+1}(F_0)e^{-i(3m+1)\varphi_2^{2\omega}(t-\tau)}.$$

From these equations, it is easy to express all the variables through F_1^{ω} getting a single time-delayed equation (functional map). If one considers the variables in discrete moments of time $t_n = 2n\tau$, the functional map is reduced to the 2D iterative map,

$$F_{n+1}e^{i\varphi_{n+1}} = \beta_2 e^{i(\psi_2-\theta_0)}\sum_{m=-\infty}^{\infty} i^m J_{3m+1}(\beta_1 J_2(2F_n))$$
$$\times J_{2m+1}(F_0)e^{-i(3m+1)(\psi_1+2(\varphi_n-\theta_0))}, \tag{5}$$

where $F_n = |F_1^{\omega}(t_n)|$, $\varphi_n = \arg(F_1^{\omega}(t_n))$, $\beta_1 = 4\sqrt{2}\alpha_1\rho_1/\delta^2$, and $\beta_2 = \sqrt{2}\alpha_2\rho_2$. Such discrete iterative maps obtained from DDEs in the limit $\tau \gg 1$ are known as singular limit maps.[12]

In Eq. (5) the right-hand side has the form of infinite series that is not convenient. However, in the case $\beta_1 \ll 1$, that can be achieved by a strong signal attenuation in the coupling transmission line ($\rho_1 \ll 1$), one can retain only one term with $m=0$ in the right-hand side of Eq. (5),

$$F_{n+1}e^{i\varphi_{n+1}} = rJ_2(2F_n)e^{i(\Delta-2\varphi_n)}. \tag{6}$$

Here $r = \beta_1\beta_2 J_1(F_0)/2$, $\Delta = \psi_2 - \psi_1 + \theta_0$. Moreover, one can split Eq. (6) into the amplitude and phase parts,

$$\varphi_{n+1} = \Delta - 2\varphi_n, \tag{7}$$

$$F_{n+1} = rJ_2(2F_n). \tag{8}$$

One can see that the phase dynamics obeys the Bernoulli map that demonstrates the hyperbolic chaotic dynamics with a positive Lyapunov exponent of $\Lambda = \ln 2$. The parameters $\psi_{1,2}$, θ_0 enter Eq. (7) as the combination Δ that determines only the constant component of a signal phase shift and does not influence the dynamics. Thus, the system dynamics is defined by a single control parameter r.

III. NUMERICAL RESULTS: ITERATIVE MAP

First consider a simplified iterative map (6). Its amplitude part (8) has a fixed point $F_n=0$, that is stable at any values of r (Fig. 2). Indeed, since $J_2(2F_n) \approx F_n^2/2$ at $F_n \ll 1$, one can see that the multiplier of the fixed point is equal to
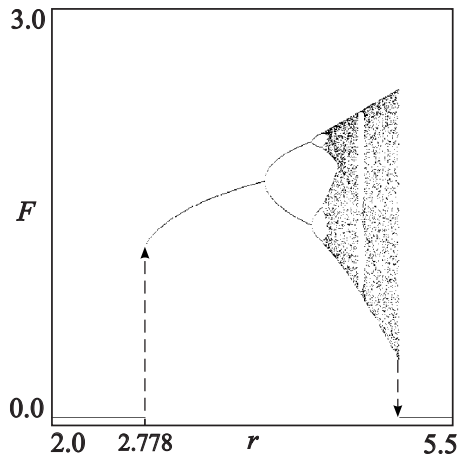
FIG. 3. The bifurcation tree for the map (8).

FIG. 4. Projections of the attractors of the map (6) on the plane of the complex variable Re F–Im F plotted at various values of r: (a) $r=2.85$, (b) $r=4.15$, (c) $r=4.3$, and (d) $r=4.6$.

zero. With the increase of r, a pair of fixed points arises via tangent bifurcation. One of these points, F_s, is stable while the other, F_u, is unstable. A bifurcation value of r is estimated analytically,

$$r_c = \frac{F^*}{J_2(2F^*)} \approx 2.778,$$

where $F^* \approx 1.15$ is the root of the equation $F^* J_2'(2F^*)/J_2(2F^*)=1$.

The stable fixed point is associated with the attractor locating on a circle. The angular coordinate of the attractor obeys the Bernoulli map. Thus, the phase dynamics is chaotic while the amplitude remains constant. This means that the oscillator generates a sequence of pulses with constant amplitude and the phase varying chaotically from pulse to pulse, similar to the systems considered in Refs. 2 and 3. An unstable fixed point is associated with an unstable invariant curve on which the dynamics of the angular coordinate is also described by the Bernoulli map. This curve serves as the boundary between areas of attraction for two coexisting attractors.

With further increase of r a sequence of period doubling bifurcations takes place and at $r \approx 4.4$ transition to chaos occurs. Now not only the phase, but also the amplitude of the signal varies chaotically. At $r=r_c \approx 5.02$ the attractor collapses with the border of its attraction basin resulting in the oscillation failure. Recall that this attractor always coexists with the stable zero fixed point. In Fig. 3 the bifurcation tree is shown illustrating the behavior picture described above.

In Fig. 4 projections of the attractors of the map (6) on the plane of a complex variable F_n are shown illustrating the period doubling scenario. The parameter Δ defines only a constant component of phase shift and has no significant influence on the dynamics of the system. Therefore, further all figures are plotted at $\Delta = \pi$ when a constant component of phase shift is equal to zero. The chaotic attractor in the F_n plane in the regime of the cycle of period 1 looks like a cycle, in the regime of the cycle of period 2 as a double cycle, etc., while the phase dynamics is always described by the Bernoulli map (Fig. 5).
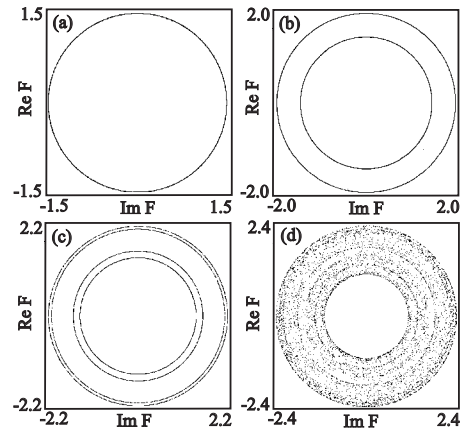
To confirm the hyperbolicity of the attractor we have calculated the Lyapunov exponents. As known, the uniformly hyperbolic attractors are structurally stable. It means that a variation of parameters, or functions, in the definition of the evolution operator does not destroy the intrinsic topology of the set of trajectories in the phase space as the perturbation is not too large. A more precise formulation is as follows.[1] For the perturbations small in the class of continuous functions with first derivatives (of class C1), the system allows reduction to the original form by a homeomorphism that is a continuous invertible change of variables (of class C0). In other words, the modified system is topologically equivalent to the original one. The Lyapunov exponents, generally speaking, are not invariant under the mentioned variable change, which is continuous, but not necessarily smooth. (Indeed, they are obtained from the variational equations derived from linearization near the reference trajectory, which implies the use of the differentiation.) Nevertheless, due to the structural stability, one can expect that the variation of the Lyapunov exponents will be as small as the perturbation; in particular, the largest exponent remains strictly positive while the topological equivalence takes place. In our case, it is supposed that by a variable change the dynamics on the hyperbolic attractor is reducible to that associated with the expanding circle
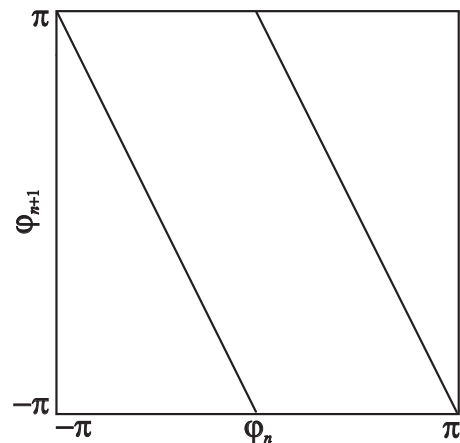
FIG. 5. The iterative diagram for the phase φ_n.

TABLE I. Spectrum of Lyapunov exponents for the map (6) at various values of r.

$r=2.85$	$r=4.15$	$r=4.3$	$r=4.6$
$\Lambda_1=0.692$	$\Lambda_1=0.692$	$\Lambda_1=0.692$	$\Lambda_1=0.692$
$\Lambda_2=-0.492$	$\Lambda_2=-0.410$	$\Lambda_2=-0.324$	$\Lambda_2=0.269$

TABLE II. Lyapunov exponents for the map (5) at $\beta_1=0.25$ and various values of β_2.

$\beta_2=39.2$	$\beta_2=57.1$	$\beta_2=59.1$	$\beta_2=63.3$
$\Lambda_1=0.690$	$\Lambda_1=0.690$	$\Lambda_1=0.692$	$\Lambda_1=0.691$
$\Lambda_2=-0.479$	$\Lambda_2=-0.310$	$\Lambda_2=-0.063$	$\Lambda_2=0.346$
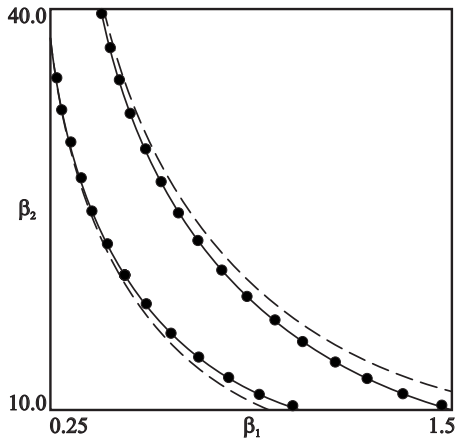
FIG. 6. The borders of the areas of the hyperbolic chaos for a map (5) taking into account two (circles) and five (solid lines) terms of a series. Dashed lines are the borders for the map (6).
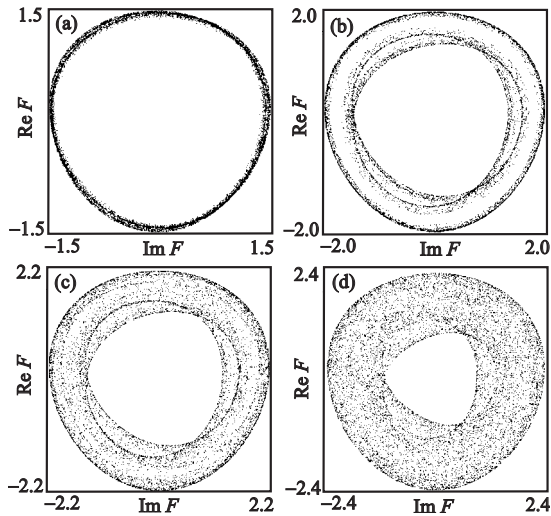
FIG. 7. The projections of attractors of the map (5) on the Re F−Im F plane plotted at various values of β_2: (a) $\beta_2=39.2$, (b) 57.1, (c) 59.1, and (d) 63.2.
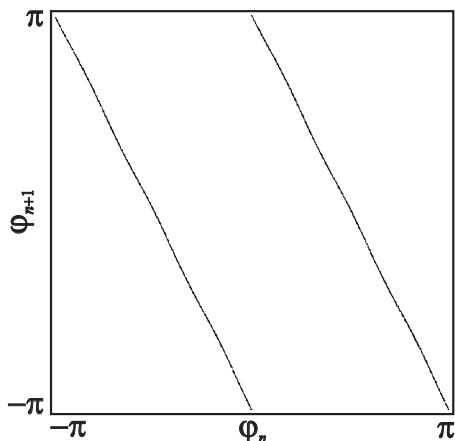
FIG. 8. The iterative diagram for the phase φ_n.

map for the angular coordinate along the attractor with expansion factor of 2. Hence, the largest Lyapunov exponent has to remain close to the constant value ln 2.

Calculations of the spectrum of Lyapunov exponents for different values of the control parameter r show that the largest Lyapunov exponent is really nearly independent of the parameter and approximately equals to ln 2 (Table I). At $r>4.4$, when the dynamics of the amplitude is also chaotic, there are two positive Lyapunov exponents, i.e., the hyperchaos regime is established.

Now consider the dynamics of the more rigorous model (5) when amplitude and phase of the signal are inseparable. Proceeding from the results mentioned above, choose $F_0=1.84$ when $J_1(F_0)$ reaches maximum, and suppose $\Delta =\psi_2-\psi_1+\theta_0=\pi$. Let us study the dynamics of the map with variation of the parameters $\beta_{1,2}$. Figure 6 shows the domain of chaotic dynamics on the (β_1,β_2) plane. Since the Bessel functions at small values of the argument rapidly decreases with increase of the order, usually it is enough to retain in Eq. (5) only two terms with numbers $m=0$ and -1. In Fig. 6 the borders of the chaos domain are plotted taking into account five terms with $m=0;\pm1;\pm2$ (solid lines) and two terms (circles) coinciding with each other. Also, in Fig. 6 the borders of chaos calculated for the simplified map (6) are presented (dashes). Since for the map (6) the borders are defined by $r=$const, on the (β_1,β_2) plane they are represented by hyperbolas. One can see that the borders for both maps are very close to each other; the lesser β_1, the better the agreement. Outside the chaotic domain, one observes the decay of oscillations, since the only one existing attractor is the stable fixed point at the origin.

Figure 7 shows projections of the attractors of the map (5) in the Re F−Im F plane plotted at $\beta_1=0.25$ and the various values of β_2. The values of β_2 are chosen so that the parameter r takes on the same values as in Fig. 4. As well as for the simplified map (6), the phase dynamics for all cases is qualitatively the same as for Bernoulli map (Fig. 8); however, a small distortion of the iterative curves is observed that occurs due to contribution of the term with $m=-1$. The more β_1, the stronger this contribution and the stronger the distortion of iterative curves. However, due to coupling between the amplitude and phase dynamics, now we cannot observe period doubling bifurcations, which occur for the simplified model (6) (cf. Fig. 4).

In Table II the values of the Lyapunov exponents are listed for different values of β_2. Similar to Eq. (6), the largest Lyapunov exponent is almost independent of the control parameter. With the increase of β_2 the second Lyapunov exponent becomes positive. The values of $\Lambda_{1,2}$ for Eqs. (5) and (6) are rather close.
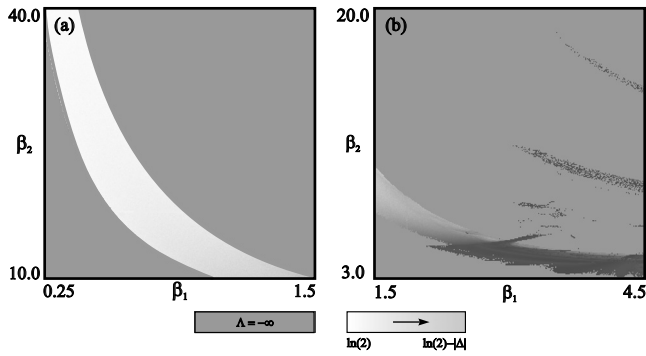
FIG. 9. Charts of the largest Lyapunov exponent for the map (5) on the (β_1, β_2) plane.

FIG. 10. The domain of hyperbolic chaos for a DDE system (1)–(4) (shaded) and for the map (5) (dashed lines) on the (β_1, β_2) plane.

Figure 9(a) shows the chart of the largest Lyapunov exponent Λ_1 on a (β_1, β_2) plane. Here the values Λ_1 are encoded by grayscale, white color corresponds to the theoretical value for the Bernoulli map $\Lambda_1 = \ln 2$. In the chaotic domain the largest Lyapunov exponent is almost constant; however, it smoothly decreases with the increase of β_1 that is associated with increasing contribution of the term with number $m = -1$. Outside the chaos domain there exists only single fixed point attractor in the origin. Since its multiplier is equal to zero, the largest Lyapunov exponent $\Lambda = \ln \mu = -\infty$. However, when the value of β_1 becomes sufficiently large, the contribution of term with $m = -1$ becomes significant and the hyperbolicity condition disrupts. In Fig. 9(b) the chart of the largest Lyapunov exponent is plotted for greater values of β_1 then in Fig. 9(a). In this computation five terms of the series in Eq. (5) were taken into account. The results reveal violation of the hyperbolicity for $\beta_1 > \beta_{max} \sim 2$.

IV. NUMERICAL RESULTS: DELAYED-DIFFERENTIAL EQUATIONS

Since the singular limit map is only an approximate model for qualitative description of the DDE behavior, we perform numerical integration of the system (1)–(4) using the fourth-order Runge–Kutta method adopted for DDEs.[13] According to the results of numerical simulations of a simplified map (5) (Sec. III), we take into account only two terms with numbers $m = 0, -1$ of infinite series in Eq. (4) that is enough in the region of parameters where the hyperbolic chaos exists.

Similar to Sec. III, we choose $F_0 = 1.84$ and $\Delta = \psi_2 - \psi_1 + \theta_0 = \pi$. The calculations show that the parameters $\psi_{1,2}$ and θ_0 do not influence strongly the dynamics of the system and define only a constant component of phase shift, as was observed above for the iterative maps. The values of other parameters approximately correspond to the parameters of the millimeter band oscillators described in Refs. 11 and 14. Suppose that the second harmonic cavity is designed by the scale-down of the fundamental frequency cavity and using well-known formulas for the cavity Q-factor,[15] one can estimate $\delta = 2\sqrt{2}$.

As shown in Sec. III, for generation of hyperbolic chaos the signal of second harmonic in the second klystron input cavity should be sufficiently small. Therefore, we choose the
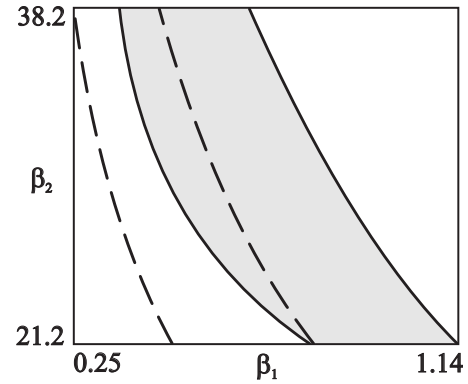
attenuation parameters in the transmission lines as $\rho_1 = 0.1$, $\rho_2 = 1.0$, and investigate the dynamics of the generator depending on the excitation parameters $\alpha_{1,2}$. In the simulations we tried different shapes of the third harmonic pulses: rectangular pulses, pulses with smoothed fronts, and $\cos^2(t/T)$ pulses. The results are quite similar for all cases; thus, further the results for the case of rectangular pulses are shown. The pulse length was chosen equal to $0.35T$, where T is the pulse-repetition interval. Due to finite transient time of oscillation build-up in the cavities, the pulse-repetition interval should slightly exceed 2τ.

The results of numerical simulation show that the dynamics of a system (1)–(4) is qualitatively similar to the dynamics of the map (5) if the pulse-repetition period of the reference signal exceeds the transit time of oscillation build-up in the cavities. In the used normalized variables the transit time is ~ 1 for cavities of the first harmonic and $\sim \delta$ for the second harmonic cavities. The pulse-repetition interval is determined by the delay time τ, which can be made as large as is needed by including the additional delays in the coupling transmission lines. Further we take $\tau = 5$ that is large enough to provide generation of hyperbolic chaos.

In Fig. 10, the domain of hyperbolic chaos on the (β_1, β_2) plane for the system (1)–(4) is shown. Also the borders of hyperbolic chaos for the map (5) are shown by dashed lines. Good qualitative agreement of the results for both models is observed in rather wide range of parameters. In Fig. 11, the plots of largest Lyapunov exponent of the hyperbolic attractor versus α_1 for two different values of α_2 are shown. For comparison with the results of Sec. III, we calculated the Lyapunov exponent for the stroboscopic Poincaré map $(t = nT)$. The largest Lyapunov exponent is almost independent from the parameter and approximately equal to $\ln 2$ that indicates structural stability of the chaotic attractor.

Figure 12 shows the typical waveform of the amplitude in the input cavity of the first klystron in the regime of hyperbolic chaos. One can see that the signal has the form of pulse sequence with nearly constant amplitude. However, the phase of the signal varies irregularly from pulse to pulse[2,3] providing robust chaotic signal. This is confirmed by Fig. 13 where typical examples of iterative diagram for the phase of subsequent pulses and projection of the attractor onto the
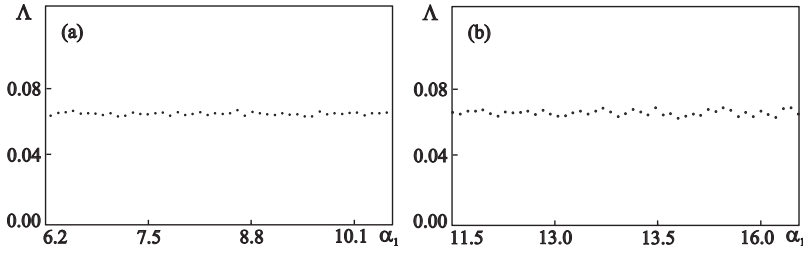
FIG. 11. Largest Lyapunov exponents of the hyperbolic attractor vs α_1 at different values of α_2: (a) $\alpha_2=23.0$ and (b) $\alpha_2=15.0$.

Re F_1^ω − Im F_1^ω plane are presented. For this plots we take the values of the variables at the moments of time when the amplitude $|F_1^\omega|$ reaches its local maximum. The plots in Fig. 13 are similar to those obtained for the iterative map [cf. Figs. 7(a) and 8]. With the increase of β_1 projection of the attractor on F_1^ω, complex plane exhibits similar transformations, as shown in Fig. 7. The attractor has a topology of the Smale–Williams solenoid, which is typical for the systems with hyperbolic chaos.

V. SUMMARY

In this paper, we present the results of detailed numerical simulation of the klystron-type microwave oscillator capable to generate signal possessing main features of hyperbolic chaos. The output signal has the form of sequence of pulses with chaotic phase dynamics approximately governed by the Bernoulli map. Three kinds of mathematical models are studied: the DDE system (1)–(4), its singular limit map (5), and the simplified map (6) obtained in the approximation that the signal arriving at the input of the second klystron is small. The results of simulations for all the three models are qualitatively similar and indicate that in rather broad range of the control parameters the regime of hyperbolic chaos is observed. The chaotic attractor has a topology of the Smale–Williams solenoid. The largest Lyapunov exponent smoothly depends on parameters and is close to theoretical value for the Bernoulli map $\Lambda \approx \ln 2$ that confirms robustness of the chaotic attractor. Moreover, at certain values of parameters the second exponent becomes positive, i.e., hyperchaos arises.

Despite of the hypothesized hyperbolic nature of the chaotic attractor, the considered scheme of the generator is of interest itself, since it reveals an opportunity to obtain robust structurally stable chaos at microwave frequencies. This property is very important for possible applications in chaos-based communication and radar systems.

APPENDIX: DERIVATION OF THE BASIC EQUATIONS

A mathematical model of the proposed generator is derived similar to other klystron-type delayed feedback oscillators.[10,11] Consider the voltages in the cavities as quasi-harmonic signals with slowly varying amplitudes $V_j^{k\omega}(t) = \mathrm{Re}[A_j^{k\omega}e^{ik\omega t}]$. Henceforth, the subscripts $j=1,2$ indicate the numbers of klystron, the superscripts $k\omega$, $k=1,2,3$, correspond to the resonance frequency of the cavities. Let I_{0j}, V_{0j}, and v_{0j} denote dc beam currents, voltages, and unperturbed electron velocities of the corresponding klystron, respectively. Following the theory of klystron,[8,9] introduce bunching parameters $X_j^{k\omega}=M_j^{k\omega}|A_j^{k\omega}|\theta_{0j}/2V_{0j}$, where $M_j^{k\omega}$ are the gap modulation factors $(0<M_j^{k\omega}<1)$, $\theta_{0j}=\omega l_j/v_{0j}$ are the unperturbed electron transit angles, and l_j are the distances between the input and output cavities, $\varphi_j^{k\omega}=\arg(A_j^{k\omega})$.

In the input cavity of the first klystron, the electrons obtain velocity modulation,

$$v \approx v_{01}\left(1 + \frac{M_1^\omega|A_1^\omega|}{2V_{01}}\cos(\omega t_1 + \varphi_1^\omega)\right), \tag{A1}$$

where t_1 is the time of electron departure from the input cavity.

Integrating Eq. (A1) one can write down an expression for the phase of the electron entering the output cavity of the first klystron,

FIG. 12. Waveform of the field amplitude in the input cavity of the first klystron in the regime of hyperbolic chaos.
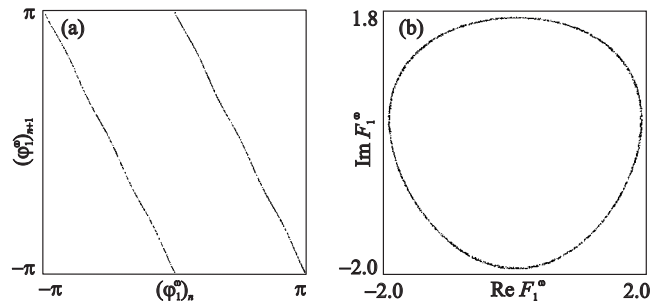
FIG. 13. The iterative diagram for the phase of the oscillations (a) and the projection of the phase portrait on Re F_1^ω − Im F_1^ω plane.

$$\omega t_2 = \omega t_1 + \theta_{01} - X_1^\omega \cos(\omega t_1 + \varphi_1^\omega), \quad (A2)$$

where t_2 is the time of electron arrival to the output cavity. Using Eq. (A2) one can obtain the complex amplitudes of the harmonics of the bunched electron current,[8,9]

$$I_1^{n\omega} = \frac{I_{01}}{\pi} \int_{-\pi}^{\pi} e^{-in\omega t_2} d(\omega t_1) = 2I_{01} J_n(nX_1^\omega) e^{-in(\theta_{01} - \varphi_1^\omega - \pi/2)}. \quad (A3)$$

Here n is the number of the harmonic. Since the output cavity is tuned to the 2ω frequency, it is excited by the second harmonic, the complex amplitude of which is

$$I_1^{2\omega} = -2I_{01} J_2(2X_1^\omega) e^{-2i(\theta_{01} - \varphi_1^\omega)}. \quad (A4)$$

From Eq. (A4) one can see that the phase of the second harmonic "inherits" the double phase of the modulation voltage $2\varphi_1^\omega$. Equations (A1)–(A4) are well known in the theory of klystrons.[8,9,16]

In the second klystron the beam is modulated by two modulating cavities. Assume that the distance between the cavities is negligible (Fig. 1). Thus, the velocity of an electron in the second klystron can be written down as follows:

$$v = v_{02}\left(1 + \frac{M_2^{2\omega}|A_2^{2\omega}|}{2V_{02}} \cos(2\omega t_1 + \varphi_2^{2\omega}) + \frac{M_2^{3\omega} A_2^{3\omega}}{2V_{02}} \cos 3\omega t_1\right). \quad (A5)$$

Integrating Eq. (A5) one can write down an expression for the phase of the electron entering in the output cavity of the second klystron,

$$\omega t_2 = \omega t_1 + \theta_{02} - X_2^{2\omega} \cos(2\omega t_1 + \varphi_2^{2\omega}) - X_2^{3\omega} \cos 3\omega t_1. \quad (A6)$$

Since the output cavity of the second klystron is tuned to a frequency of ω, it is excited by the first harmonic, the complex amplitude of which is

$$I_2^\omega = \frac{I_{02}}{\pi} \int_{-\pi}^{\pi} e^{-i(\omega t_1 + \theta_{02} - X_2^{2\omega} \sin(2\omega t_1 + \varphi_2^{2\omega} + \pi/2) - X_2^{3\omega} \sin(3\omega t_1 + \pi/2))} \times d(\omega t_1). \quad (A7)$$

Using the well-known formula $\exp(iX\sin(t)) = \sum_{k=-\infty}^{\infty} J_k(X) \exp(ikt)$,[17] we rewrite Eq. (A7) as follows:

$$I_2^\omega = \frac{I_{02}}{\pi} e^{-i\theta_{02}} \int_{-\pi}^{\pi} e^{-i\omega t_1} \sum_{n,k=-\infty}^{\infty} J_n(X_2^{3\omega}) J_k(X_2^{2\omega}) \times e^{i((2k+3n)\omega t_1 + k\varphi_2^{2\omega} + (n+k)\pi/2)} d(\omega t_1). \quad (A8)$$

In the integral all terms of series for which $2k+3n-1 \neq 0$ are equal to zero. Hence, Eq. (A8) becomes

$$I_2^\omega = 2I_{02} e^{-i\theta_{02}} \sum_{2k+3n=1} J_k(X_2^{2\omega}) J_n(X_2^{3\omega}) e^{i(k\varphi_2^{2\omega} + (n+k)\pi/2)}, \quad (A9)$$

where $k = (1-3n)/2$. Since k is an integer, n should be an odd number. Set $n = 2m+1$ ($m \in \mathbb{Z}$) that yields $k = -(3m+1)$. Then,

$$I_2^\omega = 2I_{02} e^{-i\theta_{02}} \sum_m (-i)^m J_{2m+1}(X_2^{3\omega}) J_{-(3m+1)}(X_2^{2\omega}) \times e^{-i(3m+1)\varphi_2^{2\omega}}. \quad (A10)$$

Using the property of the Bessel function $J_{-k}(X) = J_k(-X) = (-1)^k J_k(X)$,[17] the complex amplitude of the first harmonic can be written down as follows:

$$I_2^\omega = -2I_{02} e^{-i\theta_{02}} \sum_m i^m J_{3m+1}(X_2^{2\omega}) J_{2m+1}(X_2^{3\omega}) e^{-i(3m+1)\varphi_2^{2\omega}}. \quad (A11)$$

Substituting Eqs. (A4) and (A11) into the nonstationary equations of cavity excitation,[16] we obtain excitation equations of the output cavities,

$$\frac{dA_1^{2\omega}}{dt} + \frac{\omega A_1^{2\omega}}{Q_1^{2\omega}} = 2\omega K_1^{2\omega} M_1^{2\omega} I_{01} J_2(2X_1^\omega(t - l_1/v_{01})) \times e^{-2i(\theta_{01} - \varphi_1^\omega(t - l_1/v_{01}))}, \quad (A12)$$

$$\frac{dA_2^\omega}{dt} + \frac{\omega A_2^\omega}{2Q_2^\omega} = \omega K_2^\omega M_2^\omega I_{02} \sum_m i^m J_{3m+1}(X_2^{2\omega}(t - l_2/v_{02})) \times J_{2m+1}(X_2^{3\omega}) e^{-i(3m+1+\theta_{02})\varphi_2^{2\omega}}. \quad (A13)$$

Here $K_j^{k\omega}$ are the cavity shunt impedances and $Q_j^{k\omega}$ are the loaded Q-factors. Note that the right-hand sides of Eqs. (A12) and (A13) contain terms with delayed argument because of finite time of electron propagation in the drift spaces.

Following Refs. 10 and 11, we write down the equations for the input cavity excitation by the signals coming from the output cavities via the transmission lines,

$$\frac{dA_1^\omega}{dt} + \frac{\omega}{2Q_1^\omega} A_1^\omega = \frac{\omega}{2Q_2^\omega \sqrt{2}} \rho_2 e^{i\psi_2} A_2^\omega, \quad (A14)$$

$$\frac{dA_2^{2\omega}}{dt} + \frac{\omega}{Q_2^{2\omega}} A_2^{2\omega} = \frac{\sqrt{2}\omega}{Q_1^{2\omega}} \rho_1 e^{i\psi_1} A_1^{2\omega}. \quad (A15)$$

Here ρ_j and ψ_j are the attenuations and phase shifts of the output signals, respectively.

Obtain dimensionless form of Eqs. (A12)–(A15). For simplicity, assume that the parameters of both klystrons are equal, i.e., $I_{0j} = I_0$, $V_{0j} = V_0$, $\theta_{0j} = \theta_0$, etc. Introduce the normalized time $t' = \omega t / 2Q^\omega$ and the normalized complex amplitudes,

$$F_{1,2}^\omega = A_{1,2}^\omega M^\omega \theta_0 / 2V_0,$$
$$F_{1,2}^{2\omega} = A_{1,2}^{2\omega} M^{2\omega} \theta_0 / 2V_0. \quad (A16)$$

Then Eqs. (A12)–(A15) rearrange in the form (1)–(4) where

$$\alpha_1 = I_0 K^{2\omega} (M^{2\omega})^2 \theta_0 Q^\omega / 2V_0,$$
$$\alpha_2 = I_0 K^\omega (M^\omega)^2 \theta_0 Q^\omega / 2V_0 \quad (A17)$$

are the excitation parameters. In the derivation of the basic equations it was supposed that the voltage amplitudes of oscillations in the input cavities are small, $|A_1^\omega|, |A_2^{2\omega}| \ll V_0$, and

the output voltage amplitudes do not exceed the accelerating voltage, $|A_1^{2\omega}|$, $|A_2^{\omega}| \le V_0$, otherwise backward motion of the electrons occurs.

[1] A. Katok and B. Hasselblatt, *Introduction to the Modern Theory of Dynamical Systems* (Cambridge University Press, Cambridge, England, 1995).

[2] S. P. Kuznetsov, Phys. Rev. Lett. **95**, 144101 (2005).

[3] S. P. Kuznetsov and E. P. Seleznev, JETP **102**, 355 (2006).

[4] *Chaotic Electronics in Telecommunications*, edited by M. P. Kennedy, R. Rovatti, and G. Setti (CRC, Boca Raton, FL, 2000).

[5] K. A. Lukin, "Millimeter wave noise radar applications: theory and experiment," *The Fourth International Kharkov Symposium on Physics and Engineering of Millimeter and Sub-Millimeter Waves*, Vol. 1, pp. 68–73 (2001).

[6] V. V. Emel'yanov, S. P. Kuznetsov, and N. M. Ryskin, Tech. Phys. Lett. **35**, 773 (2009).

[7] *Power Vacuum Tubes Handbook*, edited by J. C. Whittaker (CRC, Boca Raton, FL, 2000).

[8] V. N. Shevchik, *Fundamentals of Microwave Electronics* (Pergamon, London, 1962).

[9] A. S. Guilmor, *Principles of Traveling Wave Tubes* (Artech House, Boston, 1994).

[10] B. S. Dmitriev, Yu. D. Zharkov, N. M. Ryskin, and A. M. Shigaev, J. Commun. Technol. Electron. **46**, 561 (2001).

[11] Y. M. Shin, N. M. Ryskin, J. H. Won, S. T. Han, and G. S. Park, Phys. Plasmas **13**, 033104 (2006).

[12] B. Mensour and A. Longtin, Phys. Rev. E **58**, 410 (1998).

[13] E. Hairer, S. Norsett, and G. Wanner, *Solving Ordinary Differential Equations. I. Nonstiff Problems* (Springer, Berlin, 1993).

[14] Y. M. Shin, J. K. So, S. T. Han, K. H. Jang, and G. S. Park, Appl. Phys. Lett. **88**, 091916 (2006).

[15] J. A. Kong, *Electromagnetic Wave Theory* (EMW, Cambridge, MA, 2008).

[16] L. A. Vainshtein and V. A. Solntzev, *Lectures on VHF Electronics* (Sov. Radio, Moscow, 1973).

[17] *Handbook of Mathematical Functions with Formulas, Graphs, and Mathematical Tables*, edited by M. Abramowitz and I. A. Stegun (Dover, New York, 1972).